INSTITUTE FOR ATOMIC STUDIES

SCHOOL OF PHYSICAL SCIENCES

ISSN 0725-783X

ELECTRON SCATTERING FROM SODIUM AT INTERMEDIATE ENERGIES

J. Mitroy, I.E. McCarthy and A.T. Stelbovics

FIAS-R-177

OCTOBER 1986.

ELECTRON SCATTERING FROM SODIUM AT INTERMEDIATE ENERGIES

J. Mitroy†, I.E. McCarthy,
Institute for Atomic Studies,
The Flinders University of South Australia,
Bedford Park 5042, S.A., Australia,
and
A.T. Stelbovics,
School of Mathematical and Physical Sciences,
Murdoch University,
Murdoch 6150, W.A., Australia.

ABSTRACT

A comprehensive comparison is made between theoretical calculations and experimental data for intermediate energy (≥ 10 eV) electron scattering from sodium vapour. The theoretical predictions of coupled-channels calculations (including one, two or four channels) do not agree with experimental values of the differential cross sections for elastic scattering or the resonant 3s to 3p excitation. Increasingly-more-sophisticated calculations, incorporating electron correlations in the target states, and also including core-excited states in the close-coupling expansion, are done at a few selected energies in an attempt to isolate the cause of the discrepancies between theory and experiment. It is found that these more-sophisticated calculations give essentially the same results as the two- and four-channel calculations using Hartree-Fock wavefunctions. Comparison of the sodium high-energy elastic differential cross sections with those of neon suggests that the sodium differential cross section experiments may suffer from systematic errors. There is also disagreement, at the higher energies, between theoretical values for the scattering parameters and those that are derived from laser-excited superelastic scattering and electron photon coincidence experiments. When allowance is made for the finite acceptance angle of the electron

spectrometers used in the experiments by convoluting the theory with a function representing the distribution of electrons entering the electron spectrometer it is found that the magnitudes of the differences between theory and experiment are reduced.

† Present Address JILA, University of Colorado, Boulder Colorado 80309, U.S.A.

PACS numbers : 34.80B.

Submitted to Journal of Physics B

INTRODUCTION

The scattering of intermediate-energy electrons by alkali metal vapours, and in particular sodium, has been the subject of numerous experimental and theoretical investigations. Sodium is an interesting system with which to probe the dynamics of electron-atom collisions. The simple electronic structure of the sodium atom, with its weakly bound 3s electron outside a neon-like core, makes sodium particularly amenable to theoretical investigation. Assuming the core to be inert, we would expect that the cross sections would resemble those of hydrogen. However, this is not the case, as the sodium 3p excited state is only 2.1 eV above the 3s ground state giving sodium an enormous dipole polarisability. Consequently, the strong coupling between the 3s and 3p levels has a large effect on the characteristics of both elastic and inelastic scattering. While experiments on sodium are naturally not as simple as those performed on the inert gases, the low temperatures required to make a dimer-free sodium beam make experiments with sodium comparatively easy. Although the large amount of experimental information should allow a thorough test of the current theories for electron scattering, there has been no comprehensive theoretical investigation which looks at all the available data.

With respect to elastic scattering, there are three sets of experimental data. Gehenn and Reichert (1972) obtained unnormalised differential cross sections at angles of 25° to 150° at energies ranging from 1 to 20 eV. Teubner et al (1978) obtained absolute elastic differential cross sections (by normalising to the inelastic 3p cross section) at higher energies (54 to 217 eV) while Srivastava and Vušković (1980) also measured absolute differential cross sections at lower energies (10 to 54 eV). The experiments of Srivastava and Vušković (1980) and Teubner et al (1978) do not agree with each other at the common energy

of 54 eV. Srivastava and Vušković (1980) suggested that the reason for the discrepancy was that the experiment of Teubner et al (1978) did not correctly allow for the geometric correction factors that account for the effective size of the interaction region changing as the electron detector is rotated. Finally, Teubner et al (1986) have asserted that the data of Srivastava and Vušković (1980) suffered from numerous systematic errors, for instance it is implied that Srivastava and Vušković (1980) have not correctly determined the angles at which the differential cross section was measured

A similar situation exists in relation to the differential cross section for the resonance transition to the 3p state. The experimental results of Srivastava and Vušković (1980) are again in poor agreement with the data of Buckman and Teubner (1979a). The differential cross sections measured by Shuttleworth et al (1975) are confined to low angles. They agree with Buckman and Teubner (1979a), but not with Srivastava and Vušković. The large discrepancies between theory and experiment are, however, at large angles. These experiments were placed on an absolute scale by using a generalised oscillator strength formalism to normalise the results. Buckman and Teubner (1979a) integrated their differential cross sections to obtain total cross sections. More recently, Teubner et al (1986) remeasured the 3s to 3p dfferential cross section at 54.4 eV and reported new measurements at 22.1 eV. The new measurements are in agreement with the earlier data of Buckman and Teubner (1979a).

Total cross sections for the 3s to 3p transition have also been measured by Enemark and Gallagher (1972) and Zapesochnyi et al (1975) Both these experiments determined the cross section by measuring the intensity of light emitted from the 3p to 3s decay. The cross sections were placed on an absolute scale by normalising to the first Born approximation at high energy.

There have also been experiments which reveal information about the

phase of the scattering amplitudes as well as the absolute magnitude. Hermann et al (1977, 1980) studied electron super elastic scattering from a laser-excited sodium beam as a function of the laser polarisation to deduce information about the scattering amplitude phase. There have also been a series of experiments which are essentially the time-reversed analogues of the experiments on laser-excited atoms. The group at Flinders University have completed a series of experiments measuring the polarisation of the emitted radiation from the excited state in coincidence with the scattered electron. These experiments also expose information about the phase of the scattering amplitude. The original work of Buckman and Teubner (1979b) measured the P_1 and P_3 polarisation components at a number of scattering angles at an energy of 100 eV. Unfortunately, there were some errors in analysis of the data which led to incorrect scattering parameters being obtained. These errors were corrected in the work of Teubner et al (1985) which determined P_1, P_2 and P_3 at an energy of 100 eV. Experiments to determine the P_1 components, and in a few instances the P_2, P_3 and P_4 components at a number of angles for energies of 12.1, 22.1, 30.0 and 54.4 eV have also been reported by Teubner et al (1986) and Riley et al (1985, 1986). All the electron-photon coincidence experiments have been performed using essentially the same system. For the purposes of brevity we will not refer to the individual papers when citing the results of this series of experiments. Rather we will refer collectively to these experiments and attribute them to the Flinders University group.

There have also been a large number of calculations completed on the sodium system. Two calculations based on distorted-wave approximations have been performed. Teubner et al (1978) report elastic cross sections calculated with a second order optical potential, in apparently good agreement with the experiment at higher energies. The Distorted Wave Polarized Orbital (DWPO) of Kennedy et al (1977) has also been applied to

electron-sodium scattering. Approximate close-coupling calculations have also been reported by Barnes et al (1965), Korff et al (1970) and Carse (1972). All these calculations neglect some part of the interaction; for instance the exchange interaction has been omitted in all these calculations. Furthermore, Barnes et al (1965) neglect the core potential while Korff et al (1970) represent the core with a Coulomb potential. We will not detail the results of these cruder models except in those cases where they are directly relevant, since all of these calculations make additional approximations beyond the truncation of the close-coupling expansion and so can be regarded as approximations to the calculations presented herein.

The close-coupling equations were solved in a two state model by Norcross (1971) and by Moores and Norcross (1972) for a four-state expansion. These authors did not make any drastic approximations to facilitate the calculations although solutions were restricted to low energies. McCarthy et al (1985) also solved the close-coupling equations in a 4-state approximation for the alkali atoms (including hydrogen) at the common energy of about 54.4 eV. In this paper large discrepancies were reported between theory and experiment for the sodium elastic and resonance inelastic differential cross sections at backward angles. It was suggested by McCarthy et al (1985) that a possible cause of the discrepancy was the use of Hartree-Fock wavefunctions to approximate the N-electron channel wavefunctions.

In this paper, we present the results of coupled-channel calculations for both elastic and inelastic scattering at energies between 10 and 217 eV. Elastic and inelastic differential cross sections as well as values for the Stokes parameters are presented and compared with experiment. It was not possible to get agreement with experimental cross sections at either low or high energies. It is found that as the complexity of the calculation is increased the results for the higher-incident-energy

electrons do not change to any significant degree. Calculations of elastic scattering for neon are also done in an attempt to isolate the cause of the discrepancy. The calculated large-angle cross sections for sodium and neon are similar. They agree with experimental cross sections for neon, but not for sodium. This suggests that the differential cross section data of Teubner et al (1978) could suffer from some unknown systematic error.

THEORY

We are interested in solving the (P-space) multi-channel Lippmann Schwinger equation (for electron-atom scattering)

$$\langle\phi_i,\underline{k}|T|\phi_j,\underline{k}'\rangle = \langle\phi_i,\underline{k}|V^{(Q)}|\phi_j,\underline{k}'\rangle \qquad (1)$$

$$+ \Sigma_\ell \int d^3k'' \langle\phi_i,\underline{k}|V^{(Q)}|\phi_\ell,\underline{k}''\rangle[E^{(+)} - \varepsilon_\ell - \tfrac{1}{2}k''^2]^{-1}\langle\phi_\ell,\underline{k}''|T|\phi_j,\underline{k}'\rangle,$$

where

$$\langle\phi_i,\underline{k}|T|\phi_j,\underline{k}'\rangle = \langle\phi_i,\underline{k}|V^{(Q)}|\Psi_j^{(+)}(\underline{k}')\rangle \qquad (2)$$

is the T-matrix element for the transition from the (N+1)-electron channel state $|\phi_j,\underline{k}'\rangle$ to $|\phi_i,\underline{k}\rangle$. The ket $|\Psi_j^{(+)}\rangle$ is the formally-exact solution of the (N+1)-electron Schrödinger equation with total energy $E^{(+)}$ for channel j while ε_ℓ is the energy of the N-electron target state $|\phi_\ell\rangle$. The operator $V^{(Q)}$ is written in the Feshbach formalism as the sum of the first-order potential and an optical potential, i.e.

$$V^{(Q)} = V + PVQ\frac{1}{(E^{(+)} - QHQ)}QVP \qquad (3)$$

The optical potential is usually included to allow for the possibility of a transition from $|\phi_j\rangle$ to $|\phi_i\rangle$ via those states excluded (Q-space) from the explicitly-coupled channel space (i.e. P-space). In the calculations presented here no optical potential is used since the the sodium system is dominated by excitations to the 3p state. The polarisation potential is dominated by the excitation to the 3p state to the extent that approximately 99% of the ground state static dipole polarisability arises from the excitation to the 3p state. Excitation to the 3p state also dominates the absorption potential as the cross section for exciting the 3p state is about 5 times larger than any other inelastic process, including ionisation.

We will describe in detail the formalism used to compute the partial-wave matrix elements as there the present formalism is a generalisation of

that described previously by McCarthy and Stelbovics (1983). This generalisation was necessary to reduce the time required for evaluation of the angular integrals when using large-basis configuration interaction (CI) wavefunctions to represent the target states (Scott and Burke, 1982). The most compact and efficient manner in which to evaluate the continuum matrix elements is to specify information about the target states using irreducible components of the density matrices. These density matrices should not be confused with the density matrix used to describe the polarisation characteristics of the scattered electron.

For the purposes of calculation a partial-wave expansion of the T- and V- matrix elements is performed. The partial-wave decomposition of the T-matrix element is

$$\begin{aligned}
&\langle \underline{k}';\phi_p L_p S_p M_{L_p} M_{S_p} | T | \phi_q L_q S_q M_{L_q} M_{S_q};\underline{k}'' \rangle \\
&= \Sigma_{\ell'\ell''m'm''J M_J} (\ell' m' \; L_p M_{L_p} | J M_J) \; (\ell'' m'' \; L_q M_{L_q} | J M_J) \\
&\times Y^{\ell'}_{m'}(\underline{k}') \; f^{\ell''*}_{m''}(\underline{k}'') \; \Sigma_{\mu'\mu''\, SM_S} \; T^{p\ell' JS}_{q\ell''}(k',k'') \\
&\times (1/2\; \mu' \; S_p M_{S_p} | S M_S) \; (1/2\; \mu'' \; S_q M_{S_p} | S M_S) \quad .
\end{aligned} \tag{4}$$

A similar result holds for the V-matrix elements. In the above expression J is the orbital angular momentum of the (N+1)-electron system while S denotes its spin. The quantum numbers of the N-electron state $|p\rangle$, with energy E_p, are L_p, S_p, M_{L_p} and M_{S_p}.

While the details of the construction of the CI wavefunctions are esentially irrelevant to the analysis we give here, it will be assumed that the N-electron channel states are CI wavefunctions specified in terms of a linear combination of Slater determinants. The most natural manner in which to proceed is to use the second quantized formalism.

It is useful to now introduce the single particle density matrix between the quantum states denoted by p and q as

$$\rho_{ij} = \langle p;L_pS_pM_{L_p}M_{S_p}|a_i^\dagger a_j|q;L_qS_qM_{L_q}M_{S_q}\rangle \quad . \tag{5}$$

where the labels i and j refer to the entire set of quantum numbers $(\alpha,\ell_\alpha m_\alpha \mu_\alpha)$ defining a single particle state. The operators $a_i^\dagger$ and a_j are the usual creation and annihilation operators. The index α will be used to define the orbital quantum number uniquely. If we restrict our discussion at present to operators with no spin dependence, then

$$\rho^k_{q,\alpha\beta} = \Sigma_{m_\alpha m_\beta \mu_\alpha} (-1)^{\ell_\alpha - m_\alpha} \begin{pmatrix} \ell_\alpha & k & \ell_\beta \\ -m_\alpha & q & m_\beta \end{pmatrix} \langle p|a^\dagger_{\alpha,\ell_\alpha m_\alpha \mu_\alpha} a_{\beta,\ell_\beta m_\beta \mu_\alpha}|q\rangle \quad . \tag{6}$$

The Wigner-Eckart theorem can be used to define the irreducible components of the density matrix, $\rho^k_{\alpha\beta}$, by

$$\rho^k_{q,\alpha\beta} = (-1)^{L_p - M_{L_p}} \begin{pmatrix} L_p & k & L_q \\ -M_{L_p} & q & M_{L_q} \end{pmatrix} \rho^k_{\alpha\beta} \quad . \tag{7}$$

With these definitions the first Born approximation matrix elements become

$$\langle \underline{k}';\phi_p|V|\phi_q;\underline{k}''\rangle = \frac{1}{2\pi^2 K^2} \Sigma_{\alpha\beta\lambda\nu} i^\lambda (2\lambda+1)(G^\lambda_{\alpha\beta}(K) - \delta_{\alpha\beta}\delta_{\lambda 0}) \times \langle \ell_\alpha \| \underline{C}^\lambda \| \ell_\beta \rangle \rho^\lambda_{\alpha\beta} C^{\lambda *}_\nu(\underline{K}) (-1)^{L_p - M_{L_p}} \begin{pmatrix} L_p & \lambda & L_q \\ -M_{L_p} & \nu & M_{L_q} \end{pmatrix} \tag{8}$$

where the reduced matrix element of the spherical tensor is

$$\langle \ell_\alpha \| \underline{C}^\lambda \| \ell_\beta \rangle = (-1)^{\ell_\alpha} [(2\ell_\alpha+1)(2\ell_\beta+1)]^{1/2} \begin{pmatrix} \ell_\alpha & \lambda & \ell_\beta \\ 0 & 0 & 0 \end{pmatrix} \tag{9}$$

and the momentum transfer, $\underline{K}$ is

$$\underline{K} = \underline{k}'' - \underline{k}' \quad . \tag{10}$$

The magnitude of the momentum transfer can be related to k', k" and the cosine of the angle between $\underline{k}'$ and $\underline{k}''$ by

$$K^2 = k'^2 + k''^2 - 2k'k''u \tag{11}$$

where

$$u = \frac{\underline{k}' \cdot \underline{k}''}{k' k''} \tag{12}$$

The function $G^{\lambda}_{\alpha\beta}(K)$ can be written as a rational function if Slater-type orbitals are used to represent the target orbitals.

$$G^{\lambda}_{\alpha\beta}(K) = \langle \alpha | j_{\lambda}(Kr) | \beta \rangle \tag{13}$$

The partial-wave matrix elements may be expressed as a sum of both direct and exchange terms.

$$V^{p\ell' JS}_{q\ell''} = V_d + V_e \tag{14}$$

where

$$\begin{aligned} V_d = {} & \Sigma_{\alpha\beta\lambda\lambda' j} \, i^{\lambda} \, (2\lambda+1)^{3/2} \, (2\lambda'+1) \, g^{\lambda j \lambda'}_{\alpha\beta}(k', k'') \, \langle \ell_{\alpha} \| \underline{C}^{\lambda} \| \ell_{\beta} \rangle \\ & \times \rho^{\lambda}_{\alpha\beta} \, [(2\ell'+1)(2\ell''+1)]^{1/2} \left[\frac{(2\lambda)!}{(2j)!(2\lambda-2j)!} \right]^{1/2} \begin{pmatrix} \ell' & j & \lambda' \\ 0 & 0 & 0 \end{pmatrix} \\ & \times (-1)^{\ell''+J+L_p} \begin{pmatrix} \ell'' & \lambda-j & \lambda' \\ 0 & 0 & 0 \end{pmatrix} \begin{Bmatrix} \ell'' & \lambda & \ell' \\ j & \lambda' & \lambda-j \end{Bmatrix} \begin{Bmatrix} \ell'' & L_q & J \\ L_p & \ell' & \lambda \end{Bmatrix} \end{aligned} \tag{15}$$

and

$$g^{\lambda j \lambda'}_{\alpha\beta}(k', k'') = \frac{k''^{\lambda-j} \, k'^{j}}{\pi} \int_{-1}^{1} du \, P_{\lambda'}(u) \, (G^{\lambda}_{\alpha\beta}(K) - \delta_{\lambda 0}\delta_{\alpha\beta}) \, K^{-(\lambda+2)} \tag{16}$$

The partial-wave matrix elements can also be expressed as

$$\begin{aligned} V_d = {} & \Sigma_{\lambda\alpha\beta} \, R^{\lambda}(\alpha, k', \beta, k'') \, \langle \ell_{\alpha} \| \underline{C}^{\lambda} \| \ell_{\beta} \rangle \, \langle \ell' \| \underline{C}^{\lambda} \| \ell'' \rangle \\ & \times \rho^{\lambda}_{\alpha\beta} \, (-1)^{\ell''+J+L_p} \begin{Bmatrix} \ell'' & L_q & J \\ L_p & \ell' & \lambda \end{Bmatrix} . \end{aligned} \tag{17}$$

where the radial matrix elements are

$$\begin{aligned} R^{\lambda}(\alpha, k', \beta, k'') = {} & i^{\ell''-\ell'} \, \frac{2}{\pi k' k''} \int_0^{\infty} dr_1 \, u_{\ell'}(k' r_1) \, u_{\ell''}(k'' r_1) \\ & \times \int_0^{\infty} dr_2 \, P_{\alpha}(r_2) \, P_{\beta}(r_2) \begin{pmatrix} \dfrac{r_<^{\lambda}}{r_>^{\lambda+1}} & \delta_{\lambda 0} \\ & r \end{pmatrix} \end{aligned} \tag{18}$$

The exchange matrix elements are considerably more complicated In this

case the density-matrix elements have a non-trivial spin dependence

$$\rho^{K\tau}_{\nu\sigma,\alpha\beta} = \sum_{m_\alpha m_\beta \mu_\alpha \mu_\beta} (\ell_\alpha m_\alpha \ell_\beta m_\beta | K\nu)\ (1/2\ \mu_\alpha\ 1/2\ \mu_\beta | \tau\sigma) \times (-1)^{\ell_\beta - m_\beta} (-1)^{1/2-\mu_\beta} \rho_{\alpha,\ell_\alpha m_\alpha \mu_\alpha\ \beta,\ell_\beta m_\beta \mu_\beta} \tag{19}$$

with the irreducible component, $\rho^{K\tau}_{\nu\sigma,\alpha\beta}$ defined by

$$\rho^{K\tau}_{\nu\sigma,\alpha\beta} = (-1)^{L_p - M_{L_p}} (-1)^{S_p - M_{S_p}} \begin{pmatrix} L_p & K & L_q \\ -M_{L_p} & \nu & M_{L_q} \end{pmatrix} \begin{pmatrix} S_p & \tau & S_q \\ -M_{S_p} & \sigma & M_{S_q} \end{pmatrix} \underline{\rho}^{K\tau}_{\alpha\beta} \tag{20}$$

The partial-wave exchange matrix elements now reduce to

$$\begin{aligned} V_{pq} = \sum_{\lambda K \tau \alpha\beta} & (R^\lambda(\alpha,k',k'',\beta) - Y^\lambda_{pq}(\alpha,k',k'',\beta)) \langle \ell_\alpha \| \underline{C}^\lambda \| \ell'' \rangle \langle \ell' \| \underline{C}^\lambda \| \ell_\beta \rangle \\ & \times \underline{\rho}^{K\tau}_{\alpha\beta} (-1)^{S+1/2+S_p} (2S+1)(2\tau+1)^{1/2} \begin{Bmatrix} S_p & S_q & \tau \\ 1/2 & 1/2 & S \end{Bmatrix} \\ & \times (-1)^{\ell_\alpha + L_p + K + J} (2J+1)(2K+1)^{1/2} \begin{Bmatrix} \ell' & \ell'' & K \\ \ell_\alpha & \ell_\beta & \lambda \end{Bmatrix} \begin{Bmatrix} \ell' & \ell'' & K \\ L_q & L_p & J \end{Bmatrix} \end{aligned} \tag{21}$$

The radial matrix elements in equation (21) are defined by

$$\begin{aligned} R^\lambda(\alpha,k',k'',\beta) = & i^{\ell''-\ell'} \frac{2}{\pi k' k''} \int_0^\infty dr_1 \int_0^\infty dr_2\ r_<^\lambda / r_>^{\lambda+1} \\ & \times P_\alpha(r_1)\ u_{\ell'}(k';r_2)\ u_{\ell''}(k'';r_1)\ P_\beta(r_2) \end{aligned} \tag{22}$$

and

$$\begin{aligned} Y^\lambda_{pq}(\alpha,k',k'',\beta) = & i^{\ell''-\ell'} \frac{2}{\pi k' k''} \int_0^\infty dr_1\ P_\alpha(r_1)\ u_{\ell''}(k'';r_1) \\ & \times \int_0^\infty dr_2\ u_{\ell'}(k';r_2)\ P_\beta(r_2)\ [E^{(+)} - \tfrac{1}{2}(E_p + E_q) - \tfrac{1}{2}(\epsilon_\alpha + \epsilon_\beta)] \end{aligned} \tag{23}$$

where ϵ_α is the single-particle energy for the orbital labelled by the quantum number α. The angular integrals in equation (19) are no problem to evaluate since the complexities of the multi configuration wavefunction are contained in the density-matrix elements $\rho^{K\tau}_{\alpha\beta}$ which only need to be evaluated at the start of the calculation. Once the partial-wave matrix elements (i.e. the $V^{p\ell'JS}_{q\ell''}$) have been computed, an integral equation for

the partial-wave T-matrix elements (i.e. $T^{p\ell' JS}_{q\ell''}$) can be formulated and solved using techniques described by McCarthy and Stelbovics (1983).

The transition amplitude is constructed by choosing the quantisation axis in the direction of the incident electron. It is

$$\begin{aligned}
&\langle \underline{k}' ; \phi_p L_p S_p M_{L_p} M_{S_p} | T | \phi_q L_q S_q M_{L_q} M_{S_q} ; \underline{k}'' \rangle \\
&= (4\pi)^{-1/2} \sum_{m'\ell'\ell''J} (\ell' m' \; L_p M_{L_p} | J \; M_J) \; (\ell'' 0 \; L_q M_{L_q} | J \; M_J) \; Y^{\ell'}_{m'}(\underline{k}') \\
&\times \sum_{\mu'\mu'' S} (1/2 \; \mu' \; S_p M_{S_p} | S M_S) \; (1/2 \; \mu'' \; S_q M_{S_q} | S M_S) \; - \left(T^{p\ell' JS}_{q\ell''} - V^{p\ell' JS}_{q\ell''} \right) \\
&+ \langle \underline{k}', \phi_p L_p S_p M_{L_p} M_{s_p} | V | \phi_q L_q S_q M_{L_q} M_{s_q} ; \underline{k}'' \rangle . \qquad (24)
\end{aligned}$$

We use this form for the T-matrix element to minimise any inaccuracies that may build up when a large number of partial-wave matrix elements are summed. The construction of the cross section from the T-matrix elements is detailed in McCarthy and Stelbovics (1983).

DESCRIPTION OF THE CALCULATIONS

As mentioned previously, our initial calculations (McCarthy et al 1985) on the alkali atoms were in poor agreement with experimental values for the differential cross sections. Accordingly, we have done a large number of calculations of varying complexity in an attempt to isolate the cause of the discrepancy between the theory and experiment. These different calculations are described below.

(i) FBA. The simplest realistic model for the inelastic 3s to 3p transition is the first Born approximation. This is expected to be accurate for small-angle scattering at high energies. Hartree-Fock wavefunctions were used in the evaluation of the first Born matrix element.

(ii) SE. The simplest possible model, applicable only to elastic scattering, is to solve the coupled-channels equations for just the entrance 3s channel. The resulting equations are just the static-exchange (SE) equations. The SE equations were solved for a total angular momentum (J) up to 40. The target bound state was represented by a HF wavefunction with the single-particle orbitals expressed as linear combinations of Slater-type orbitals.

(iii) CC2. The coupled-channel equations are solved for the 3s and 3p channels. A 24-point gaussian quadrature mesh is used to discretise the off-shell part of the integral equations for $J \leq 24$ for energies ≥ 30.0 eV. When the incident energy is ≤ 22.1 eV, polarisation effects are quite important for the higher partial waves and so a 24 point gaussian mesh is used for $J \leq 34$. No exchange matrix elements are computed for $J > 16$. The Unitarised Born Approximation (UBA) is used to approximate the rest of the T-matrix elements for $J \leq 80$. The first Born approximation is used for $J > 80$. HF wavefunctions are again used to represent the channel states.

(iv) CC4. The channel space is enlarged to include the 3s, 3p, 4s and 3d channels. Details of the calculation are similar to those of the CC2 calculation.

(v) FBA-CI. The influence of inadequacies in the HF wavefunctions on small-angle scattering for the 3s to 3p transition can be determined by using configuration interaction (CI) wavefunctions to evaluate first Born matrix elements. CI wavefunctions were constructed for the 3s, 3p, 3d and 4s states. Using the HF 3s, 3p, 3d, 4s and 4p configurations as a reference set, the Slater determinants that could be formed by allowing all possible single and double excitations (excluding the doubly-occupied 1s shell) from the reference configurations into the $\overline{4s}$, $\overline{4p}$ and $\overline{3d}$ pseudo-orbital space were included in the CI basis. The pseudo-orbitals were constructed by maximising their overlap with the 2p and 3s orbitals. The quality of the CI wavefunctions can be estimated by computing optical oscillator strengths for the 3s-3p transition. Using experimental energy differences to compute the oscillator strength, the length and velocity matrix elements give 0.998 and 0.916 respectively for the CI wavefunctions. The best calculation is that of Froese-Fischer (1976) which gave values of 0.964 and 0.967 for the length and velocity oscillator strengths respectively. While our calculations have not converged, the CI wavefunctions are a definite improvement over HF wavefunctions which give 1.066 and 0.927 for the length and velocity oscillator strengths respectively.

(vi) CC4-CI. These calculations are identical to the CC4 calculations apart from the fact that the CI wavefunctions used for the FBA-CI calculations were used to represent the N-electron channel states. In view of the fact that these calculations were extremely time consuming, results are presented at only a few selected energies. The details are the same as for the CC4 calculation.

and 3d

the

on

ermined

tate

for

4p

nt

l space

tructed

g

g

rength,

is that

for

hile

e a

and

ctively.

tions

BA-CI

tates.

ime

rgies.

(vii) CC5-XC. Channels involving excitation of a 2p electron are explicitly included in the close-coupling expansion. As well as the usual 3s and 3p channels, the $2p^5 3s^2\ ^2P^o$ state and the two $2p^5 3s\bar{3}d\ ^2P^o$ states were included in P-space. The excitation energies of the states with excited 2p electrons are 1.27, 2.43 and 2.61 a.u. respectively. Details of the calculation are similar to the CC2 calculation.

RESULTS FOR ELASTIC SCATTERING

Elastic differential cross sections at energies of 10 and 20 eV are depicted in figure 1. The pronounced forward peaking of the cross sections is caused by the extremely strong coupling between the 3s and 3p channels. The differences between the CC2 and CC4 calculations are relatively small, indicating that it is the coupling with the 3p state which dominates the collision. The influence of coupling to the 4s and 3d levels is most important at small angles. This is most clearly seen in table 1 where the total elastic cross section for the CC4 calculation is some 10% larger than for the CC2 calculation at 10 eV. That the theoretical cross sections do not agree with the total cross sections of Srivastava and Vušković (1980) may be partly due to the extrapolation procedure used by Srivastava and Vušković (1980) to extend their differential cross sections from 10° to 0°.

The overall agreement between the most complete theory (CC4) and the experiments of Srivastava and Vušković (1980) is not particularly good. Better agreement is obtained with the experimental results of Gehenn and Reichert (1972) where an excellent fit at 20 eV is achieved. However as the experimental data of Gehenn and Reichert (1972) were not absolute we have normalised their data to fit the theory (the CC4 calculation) at the secondary maximum. A visual inspection of the shapes of the cross sections at the energy of 20 eV clearly demonstrates that the experimental results by the different groups are not consistent with each other.

The elastic differential cross sections at the higher energies of 54.4, 100 and 150 eV are shown in figure 2. The actual experimental values depicted are not those of Teubner et al (1978). Rather we use the final values of Buckman (1979) which are slightly different. One of the features of these curves is the reasonable fit to the experimental differential cross sections obtained by Teubner et al (1978) with a second-

order optical model. However the apparently good agreement must be regarded as an artifact of their calculation since the absorptive part of their optical potential does not correspond to the physics of the electron-sodium system. In this calculation inelastic processes involving both the 3s and 2p subshells were permitted to contribute to the absorption potential. Teubner et al (1978) used the closure approximation to facilitate calculation of the optical potential. Rather than having different closure energies for the different shells, Teubner et al (1978) used a single closure energy for both the 2p and 3s shells. Such a procedure is unlikely to be valid since the HF single-particle energies for these two shells are quite different (e.g. ϵ_{2p} = 40.3 eV, ϵ_{3s} = 4.96 eV). With such a restriction it is possible that the average excitation energies of the core excited $2p^5 3snl$ levels are too small, thus causing the strength of the absorption potential to be overestimated. Unfortunately Teubner et al (1978) did not specify the value of the closure energy that was used. However using information about the absorption potential that is available in Buckman (1979), the contribution to the reaction cross section that results from excitations of electrons from the 2p subshell can be computed. Rough calculations indicate that the reaction cross section is about 10 a.u. at 100 eV. This is about 10 times larger than the total reaction cross section of neon (de Heer et al 1979) and about thirty times larger than the ionisation cross section of Na^+ (Hooper et al 1966). Since the absorptive component of the optical potential used by Teubner et al (1978) is too large (for core electrons) the smaller cross section at backward angles must be regarded as an artifact of the calculation.

None of the present calculations are in good quantitative agreement with the experimental results. While the theoretical calculations in figure 2 agree qualitatively with the experiment, in particular with the positions of the minima, the absolute values of the large-angle cross

sections are almost an order of magnitude larger than the experimental values. One of the most noticable features of figure 2 are the small differences between the SE, CC2 and CC4 calculations at backward angles. This provides quite dramatic evidence that polarisation and inelastic processes involving the outer 3s electron are unimportant for high-energy large-angle scattering. The dominant mechanism for large-angle elastic scattering at these energies is just the static interaction of the continuum electron with the sodium ground state. Given the insensitivity of the large-angle cross section to inclusion of additional channels in the close-coupling expansion the large discrepancies with experiment are somewhat puzzling. In order to unravel the possible causes for the discrepancies, particular attention will be paid to the 100 and 150 eV cross sections.

The fact that the elastic data are much smaller than the theoretical calculations at backward angles would seem to imply that reactive scattering involving excitation of the 2p electrons may be important at these angles. The present CC5-XC calculations, which explicitly include channels with excited 2p electrons were done to check this hypothesis. The results of these calculations, shown in figure 2, indicate that while absorption by the core has some influence on the large-angle cross sections, the effect is not large enough to explain the discrepancy with experiment.

Additional evidence that the core is indeed inert at these energies is provided by the results of calculations on the neon system. A simple but not inaccurate model of the sodium atom is to picture it as a weakly bound valence electron outside of a neon-like core. Since the binding energies of the neon atom are smaller than those of sodium, the neon core is easier to excite and so a comparison of static-exchange calculations for neon with more sophisticated calculations and experimental data should permit us to decide whether core excitations are important for neon and

sodium. Figure 3 depicts the results of a static-exchange calculation and an R-matrix calculation by Fon and Berrington (1981) with one pseudo state to account for polarisation and inelastic events. The experimental data of Gupta and Rees (1975a, b) and Williams and Crowe (1975) are also shown in figure 3. The static-exchange results are in excellent agreement with both the experimental data and the R-matrix calculation. This agreement provides both empirical and theoretical evidence to further support the hypothesis that core excitations are not responsible for the discrepancy between theory and experiment.

It is particularly interesting to superimpose the sodium and neon differential cross sections (figure 4) at the common energy of 150 eV. The present sodium calculations are in broad agreement with the neon experimental and theoretical cross sections. If we ignore the sodium data, the agreement between neon and sodium cross sections at large angles indicates that inner regions of the sodium and neon atoms are quite similar and that reactive scattering involving excitations of the 3s electron is not important for large angle scattering. Both of these propositions are eminently plausible and supported by the results of the calculations depicted in figures 2, 3 and 4.

Since we have eliminated the possibility that absorption by the core is the cause of the distinctions between theory and experiment there does not seem to be any way that the differences between theory and experiment can be reconciled. The hypothesis that inelastic events involving the valence 3s electron may be responsible for the differences is not supported by the comparison of the SE, CC2 and CC4 calculations where it was found that the coupling between the channels had no effect on the large-angle differential cross sections. Since coupling to the 3p, 3d and 4s channels has an insignificant effect on the large-angle elastic cross section it is unlikely that those channels which have been omitted from P space will affect the cross section at these angles.

Given the constant differences between theory and experiment at high incident energies, regardless of the sophistication of the calculations, one must question the validity of the experimental evidence. Firstly, none of the experimental measurements by the different groups are compatible with each other. Second, the various calculations of elastic scattering seem to have converged. Next, the large differences between elastic cross sections for neon and sodium at backward angles certainly seem very implausible. Until there is a greater body of convergent experiment results to suggest otherwise, we cannot rule out the possibility that differences between theory and experiment may be due to large systematic errors in the experiments.

TOTAL AND DIFFERENTIAL CROSS SECTIONS FOR THE RESONANCE TRANSITION

Total cross sections for the 3s to 3p transition are tabulated in table 2 for a variety of energies. The absolute cross sections of Enemark and Gallagher (1972) and Zapesochnyi et al (1975) are not in good agreement with each other. Some of the cross-section values attributed to Enemark and Gallagher in table 2 were obtained by interpolation. Both these sets of cross sections were placed on an absolute scale by normalising to cross sections calculated in the first Born approximation. The normalisation point for Enemark and Gallagher (1972) was at 1000 eV while 300 eV was used by Zapesochnyi et al (1975). Both Enemark and Gallagher (1972) and Zapesochnyi et al (1972) adopt semi-empirical methods, using the known value of the optical oscillator strength to calculate the first Born cross section; and so should yield total cross sections which are more trustworthy than those computed from ab-initio wavefunctions. The total cross sections of Enemark and Gallagher (1972) and Zapesochnyi et al (1975) do not agree within their quoted experimental errors. Since the oscillator strengths (length form) for the HF and CI wavefunctions used here, 1.066 and 0.998 respectively are slightly larger than the accepted value of 0.97 (Froese-Fischer 1976) it is expected that our calculations will yield first Born cross sections which are slightly too large. Given that the difference between our calculated oscillator strengths and the accepted value is less than 10%, the large difference with the total cross section of Zapesochnyi et al (1975) at 217 eV, which at this energy is the same as their first Born cross section, indicates that their first Born calculation is probably defective. On the other hand, our FBA calculations are consistent with the semi-empirical first Born cross sections used by Enemark and Gallagher (1972) to normalise their results. At high energies, our first Born approximations FBA and FBA-CI, as well as the close-coupling calculations predict cross sections

slightly larger than Enemark and Gallagher (1972). It is noticable that at high energies the theoretical cross sections for the CC2 and CC4 calculations tend to be slightly larger than the experimental values. The dominant contribution to the total cross section for the resonance transition comes from small-angle scattering. The CC4-CI calculations, which use wavefunctions giving a smaller value for the 3s to 3p oscillator strength, result in slightly smaller total cross sections which are in better agreement with experiment. At low energies the cross sections of Enemark and Gallagher (1972) are much smaller than those reported by Zapesochnyi et al (1975). The present calculations tend to lie between the results of Enemark and Gallagher (1972) and Zapeschonyi et al (1975) at low energies. Since the total cross section decreases as the number of channels is increased it would be expected that, if the number of channels were increased beyond the present maximum of four, the calculated cross section would further decrease and be in better agreement with Enemark and Gallagher (1972).

The small-angle differential cross sections shown in figure 5 give insight into the dynamics of the collision at small momentum transfers. At energies of 22.1 and 54.4 eV it is possible to distinguish between the CC2 and CC4 cross sections. At higher energies the CC2 and CC4 cross sections tend to merge. On the other hand, the FBA and CC4 cross sections are only in exact agreement at the smallest angles. We note that our best calculation, namely the CC4, agrees best with the data at all energies.

The differential cross sections at the low energies of 10, 20 and 22.1 eV are shown in figure 6. The differences between the CC2 and CC4 calculations are not very large. While there is fair agreement with the data of Srivastava and Vušković (1980) at 20 eV the agreement at 10 eV is not nearly so good. A careful comparison of the data points of Srivastava and Vušković (1980) with respect to the CC4 cross section reveals some irregularities in the data points at small angles. This scatter in the

data points could be an indication that the experiment of Srivistava and Vušković may not be absolutely reliable. At 22.1 eV, there is only fair agreement in magnitude between the CC4 calculation and the data of Teubner et al (1986) although the position of the two minima and the secondary maxima agree.

At the higher energies of 54, 100 and 150 eV (figure 7), there are large discrepancies between our CC4 calculations and the experimental data of Buckman and Teubner (1979a). The more recent data of Teubner et al (1986) at 54 eV are identical with the older cross section measurements. There is better agreement with the data of Srivastava and Vušković (1980) although this data has been the subject of massive criticism by Teubner et al (1986). In a number of respects the situation is reminiscent of that which arose with respect to elastic scattering. The calculated differential cross sections agree with the experiments in the positions of the minima but are once again an order of magnitude larger at backward angles.

At this point some mention must be made of that aspect of the work of Teubner et al (1986) in which they manipulate the data of Srivastava and Vušković (1980) with a view to resolving the discrepancies between the two sets of data. By shifting the data points of Srivastava and Vušković (1980) by +3° and renormalising their data points they find better agreement between the adjusted data of Srivastava and Vušković (1980) and their data at 54.4 eV. However, it must be noted that this agreement with the adjusted data does not extend to small angles. Teubner et al (1986) imply that the discrepancy at small angles may be due to saturation effects. There is an aspect of uncertainty in the procedure adopted by Teubner et al (1986). The analysis of the experiment of Srivastava and Vušković (1979) required that the raw data be scaled by a function accounting for changes in the interaction region as the electron beam was rotated. Since this scaling function is angle dependent, it is clear

that if the data of Srivastava and Vušković (1980) are shifted by +3°, then a further correction accounting for the change in the scaling function should be considered.

In an earlier work (McCarthy et al 1985), it was suggested that a possible cause of the discrepancies between the theoretical and experimental 3s-3p cross sections could be deficiencies in the wavefunctions used to represent the N-electron channel states. The generalised oscillator strengths resulting from HF and CI wavefunctions were found to be quite different at large values of momentum transfer. Presumably the use of more accurate CI wavefunctions would lead to differential cross sections that are more accurate at large angles. The CC4-CI calculations, which were undertaken to test the importance of using better wavefunctions, did not support this supposition. The cross sections resulting from these calculations were not shown in figures 6 and 7 because the CC4 and CC4-CI cross sections were essentially indistinguishable. The similarity of the CC4 and CC4-CI cross sections is a result of the fact that the first Born transition amplitude for the 3s-3p process is insignificant at large values of momentum transfer. The process which dominates large-angle inelastic scattering involves the continuum electron undergoing large-angle elastic scattering preceding or following the inelastic 3s-3p excitation. Consequently, even though the first Born amplitudes for CI and HF wavefunctions are different at large values of momentum transfer, the small value of the amplitude at these angles ensures that CI effects will not have an appreciable influence on the large-angle cross sections.

Once again, we have a situation in which large differences between theory and experiment still persist as the theoretical models are made increasingly sophisticated. The resolution of the problem is more complicated than for elastic scattering. Since large-angle inelastic scattering is predominantly the result of a two-step process accurate

calculation of the differential cross section in this angular range is inherently more difficult. Nevertheless it is very difficult to understand how both the elastic and inelastic differential cross sections should be too large at backward angles. The smaller elastic cross section given by the data of Teubner et al (1978) would imply increased reactive scattering at backward angles and a larger inelastic cross section. The recent experiment of Teubner et al (1986) does not resolve the situation since the apparatus used is essentially a modified version of the apparatus used by Buckman and Teubner (1979a). In summary, it would be fair to state that an impasse currently exists in the comparison between the most sophisticated calculations and the current experimental data for sodium.

STOKES PARAMETERS FOR THE RESONANCE TRANSITION

Two essentially different experiments have been done. The experiments performed by the Flinders University group have measured the polarisation components of the emitted radiation (i.e. the Stokes parameters) in coincidence with the inelastically scattered electron. The polarisation components of the light being emitted perpendicular to the scattering plane are

$$P_1 = \frac{I(0°) - I(90°)}{I(0°) + I(90°)}$$

$$P_2 = \frac{I(45°) - I(135°)}{I(45°) + I(135°)} \qquad (25)$$

$$P_3 = \frac{I(RHC) - I(LHC)}{I(RHC) + I(LHC)}$$

It is also possible to measure the polarisation of the light being emitted parallel to the scattering plane. The only component so far measured is P_4 which is

$$P_4 = \frac{I(0°) - I(90°)}{I(0°) + I(90°)} \qquad (26)$$

In the above equations, $I(\alpha)$ is the number of coincidence events when the optical axis of the polariser makes an angle α with the incident beam direction. I(RHC) and I(LHC) measure the right and left polarisation components respectively. The Stokes parameters can be expressed in terms of the collision-frame density-matrix elements (Hermann and Hertel 1982a, 1982b, Teubner et al 1985) as

$$P_1 = 0.141\ (1 - 4\rho_{11})$$

$$P_2 = 0.40\ \mathrm{Re}\ \rho_{10}$$

$$P_3 = 1.577\ \mathrm{Im}\ \rho_{10} \qquad (27)$$

$$P_4 = \frac{0.5922\ (2\rho_{11} - 1)}{4.395 - 1.184\ \rho_{11}}$$

where the spin averaged density-matrix elements expressed in terms of T matrix elements are

$$\rho_{mm'} = \frac{\frac{1}{4}T_m(0)T_{m'}(0)^* + \frac{3}{4}T_m(1)T_{m'}(1)^*}{\Sigma_m\left[\frac{1}{4}T_m(0)T_m(0)^* + \frac{3}{4}T_m(1)T_m(1)^*\right]} \qquad (28)$$

The superscripts (0) and (1) denote the spin quantum number of the (N+1)-electron system. In deriving the above expressions it was assumed that the scattering amplitudes obey reflection symmetry about the scattering plane (i.e. $\rho_{11} = \rho_{1-1}$). This identity is satisfied as long as spin-orbit interactions can be neglected. This is expected to be the case for a low Z atom like sodium. One consequence of this is that both P_1 and P_4 are functions of only ρ_{11}, hence P_1 can be expressed in terms of P_4 using

$$P_1 = (1.859P_4 - 0.141)/(1 - P_4) \quad . \qquad (29)$$

Rather than comparing P_4 separately with theory, we have transformed those values of P_4 that are available into equivalent P_1 values. There are a number of alternative ways to parameterise the information about the scattering amplitudes that is inherent in the Stokes parameters. We have taken the view that it is best to present our results in terms of P_1, P_2, P_3 and P_4 since these are the quantities that are actually measured in the experiments of the Flinders University group. The quantities measured in the experiments of Hermann et al (1977, 1980) are easily expressed in terms of Stokes parameters.

There is one other parameter which gives useful information about the reaction dynamics. This is the reduced polarization, $|\tilde{P}|$ defined by

$$|\tilde{P}| \quad \left[\left(\frac{P_1}{0.141}\right)^2 + \left(\frac{P_2}{0.141}\right)^2 + \left(\frac{P_3}{0.558}\right)^2\right] \qquad (30)$$

When $|\bar{P}| = 1$, the singlet and triplet scattering amplitudes are parallel and the excitation can be characterised as "coherent". In all those instances for which we present values for P_1, P_2 and P_3 it was found that $|\bar{P}|$ was ≥ 0.98.

When analysing the experimental data which yield information on the scattering parameters it is important to make sure that our analysis corresponds to the exact experimental situation. The experiments allegedly give the scattering parameters as a function of the electron scattering angle. However, what is really measured in these experiments (at any angle) are the scattering parameters weighted by the differential cross section averaged over the finite angular resolution (i.e. instrument function) of the electron spectrometer. Consequently, when comparing with experiment the theoretical parameters should be turned into an angular average by folding the theory with the differential cross section and a function $h(\theta)$ representing the angular distribution of the electrons entering the electron spectrometer. For example, one should not compare $P_1(\theta)$ with experiment, rather one should compare $\langle P_1(\theta)\rangle$, defined by

$$\langle P_1(\theta)\rangle = \frac{\int_{\theta-\delta\theta}^{\theta+\delta\theta} d\phi\ h(\phi)\ P_1(\phi)\ \frac{d\sigma(\phi)}{d\Omega}}{\int_{\theta-\delta\theta}^{\theta+\delta\theta} d\phi\ h(\phi)\ \frac{d\sigma(\phi)}{d\Omega}} \qquad (31)$$

with the experiment. It is straightforward to demonstrate that the finite angular resolution of the electron spectrometer can have a considerable influence on the value of polarisation that is actually measured. At high electron energies, where the differential cross section is extremely forward peaked, there will be a preferential weighting towards low angles when the average polarisation component given by equation (31) is computed. The Flinders University group do not give any information about the angular resolution of their electron spectrometer. Hermann et al (1977) do not give any information about the acceptance angle of their electron spectrometer although the error bars seem to indicate a half

width of about ±2.5°. The angular resolution in the experiment performed by Hermann et al (1980) is quoted as ±1°. We have done calculations to test the potential importance of finite angular resolution by folding the CC4 calculations with a spectrometer function with a half-width of ±2.1°. We will refer to the CC4 calculation which has been convoluted as the <CC4> calculation.

Values for P_1 are depicted as a function of scattering angle at electron energies of 12.1, 22.1 and 30 eV in figure 8. An interesting feature of these results is that as the energy increases the first Born approximation gives results which are quite similar to the CC2 and the CC4 results. At 30 eV the CC2 and CC4 calculations give identical results and are very hard to distinguish from the FBA results. The importance of folding the calculated P_1 with a detector function is confirmed by the curve showing the results of the CC4 calculation convoluted with a detector function. The differences between the FBA and CC4 calculations at 30 eV are smaller than the differences between the <CC4> and CC4 curves.

At the higher energies of 54.4 and 100 eV the theoretical values of the different calculations of P_1 (figure 9) seem to be converging. We would intuitively expect that this would be the case since the approximations implicit in using a finite-channel close-coupling calculation should be more realistic at high energies than at low energies. However it is much more important to convolute the calculated P_1 with a detector function at these energies since both P_1 and the differential cross section vary extremely rapidly with the electron scattering angle. This is certainly apparent in figure 9 where it is seen that convoluting the calculated P_1 values leads to large changes which bring the theory into better accord with the experimental data.

Values of the parameter P_2 are shown in figure 10 at energies of

12.1, 22.1 and 100 eV. The agreement between theory and experiment is reasonable at the low energies of 12.1 and 22.1 eV. At 100 eV, the data of Teubner et al (1985) cannot be reconciled with the calculations. Although the theory here is sensitive to resolution effects, the <CC4> calculation is not in any better agreement with the data than the CC4 calculation. With regard to the theoretical calculations it is interesting to note that differences between the FBA, CC2 and CC4 calculations still persist at 100 eV at angles greater than 2°.

Values for the polarisation component P_3 at energies of 12.1, 22.1 and 100 eV are shown in figure 11. This parameter is quite a sensitive test of the theory since the first Born approximation predicts that P_3 should be zero for all scattering angles. The theoretical values of P_3 are roughly proportional to the scattering angle for all energies and angles considered. The data of Hermann et al (1980) and the 12.1 eV data of the Flinders group are consistent with this trend although detailed agreement is not achieved. On the other hand, the 100 eV P_3 data points of Teubner et al (1985) do not follow any obvious trend although they straddle the theoretical results. It is clear that the error bars associated with the measurements of Teubner et al (1985) are somewhat optimistic. The <CC4> calculation of P_3 shows that this parameter is not particularly sensitive to angular resolution effects, even at 100 eV. This is due to the fact that P_3 does not vary as rapidly with scattering angle as do P_1 and P_2. Hence, if the object of an experiment is to provide a detailed test of the theory, we believe that P_3 is the best polarisation component to measure. It is the most sensitive of the Stokes parameters to the degree of sophistication of the calculation and least sensitive to the potential distortions induced by the finite size of the electron spectrometer.

CONCLUSIONS

Although our calculations reproduce the general trends of the experimental data in all instances, exact quantitative agreement with experiment has not been achieved. In a number of instances where there are discrepancies between theory and experiment, experiments performed by different groups are also in conflict. With respect to the differential cross section data, the overall consistency of the different calculations, and the agreement of sodium and neon elastic scattering calculations with elastic neon cross sections, tends to suggest that the differential cross section experiments suffer severely from the effects of systematic errors. There also appear to be problems with the measurements of the Stokes parameters. While it has often been stated that determination of the correlation and coherence parameters provides a much more discriminating test of any theory than does the determination of the differential cross section, in the particular case of sodium at the energies we have considered, we do not believe that the present experiments are of sufficient quality to provide a really detailed test of the theory. At high energies like 100 eV, inclusion of angular resolution effects is of great importance and must be considered in any future work.

In view of the confused situation with regard to experimental determination of the total and differential cross sections (as well as the Stokes parameters) we believe that it is premature to suggest that the disagreements between theory and experiment are due to theoretical deficiencies. There is clearly a need for further experiments to be carried out in order to clarify the situation.

ACKNOWLEDGMENTS

We must thank those members of the Flinders University group who let us examine their data prior to publication. We also would like to thank Dr. I. Afnan for an interesting and helpful discussion. We acknowledge the financial support provided by the Australian Research Grants Scheme.

REFERENCES

Barnes L L, Lane N F and Lin C C, 1965 Phys.Rev. 137A 388.

Bransden B H and McDowell M R C, 1977 Phys.Rep. 30 207.

Bransden B H and McDowell M R C, 1978 Phys.Rep. 46 249.

Buckman S J 1979 Ph.D. Thesis Flinders University.

Buckman S J and Teubner P J O, 1979a J.Phys.B 12 1741.

Buckman S J and Teubner P J O, 1979b J.Phys.B 12 L583.

Carse G, 1972 J.Phys.B 5 1928.

Enemark E A and Gallagher A, 1972 Phys.Rev.A 7 1573.

Fon W C and Berrington K A, 1981 J.Phys.B 14 323.

Froese Fischer C, 1976 Can.J.Phys. 54 1465.

Gehenn W and Reichert E, 1972 Z.Phys.A 254 28.

Gupta S C and Rees J A, 1975a J.Phys.B 8 417.

Gupta S C and Rees J A, 1975b J.Phys.B 8 1267.

de Heer F J, Jansen R H J and van der Kaay W 1979 J.Phys.B 12 979.

Hermann H W, Hertel I V, 1982a Comments At.Mol.Phys. 12 61.

Hermann H W, Hertel I V, 1982b Comments At.Mol.Phys. 12 127.

Hermann H W, Hertel I V and Kelley M H, 1980 J.Phys.B 13 3465.

Hermann H W, Hertel I V, Reiland W, Stamatovic A and Stoll W, 1977 J.Phys.B 10 251.

Hooper J W, Lineberger W C and Bacon F M, 1966 Phys.Rev. 141 165.

Kennedy J V, McDowell M R C and Myerscough V I, 1977 J.Phys.B 10 3795.

Korff D F, Chung S and Lin C C, Phys.Rev.A 1970 545.

McCarthy I E, Mitroy J and Stelbovics A T, 1985 J.Phys.B 18 2509.

McCarthy I E and Stelbovics A T, 1983 Phys.Rev.A 28 2693.

Moores D L and Norcross D W, 1972 J.Phys.B 5 1482.

Norcross D W, 1971 J.Phys.B 4 1458.

Riley J L, Teubner P J O and Brunger M J, 1985 Phys.Rev.A 31 1959.

Riley J L, Teubner P J O and Brunger M J, 1986 J.Phys.B 19 129.

Scott N S and Burke P G, 1982 Comp.Phys.Commun. 26 419.

Srivastava S K and Vušković L, 1980 J.Phys.B 13 2633.

Shuttleworth T, Newell W R and Smith S C H, 1977 J.Phys.B 10 1641.

Teubner P J O, Buckman S J and Noble C J, 1978 J.Phys.B 11 2345.

Teubner P J O, Riley J L, Furst J E and Buckman S J, 1985 J.Phys.B 18 351.

Teubner P J O, Riley J L, Brunger M J and Buckman S J, 1986 J.Phys.B 19 (to be published).

Williams J F and Crowe A, 1975 J.Phys.B 8 2233.

Zapesochnyi I P, Postoi E M and Aleksakhin I S, 1975 Sov.Phys.JETP 41 865.

Table 1. Total cross sections (in a_0^2) for elastic scattering as a function of energy. The only experimental results are those of Srivastava and Vušković (1980) which are in the row denoted SV.

E(eV)	10	20	22.1	54.4	100	150	217
CC1	25.0	19.5	19.3	17.2	13.4	10.7	8.40
CC2	59.0	27.6	25.8	17.5	13.4	10.6	8.36
CC4	64.2	28.9	26.8	17.6	13.2	10.6	8.31
CC4-CI	--	--	25.9	17.2	--	10.6	--
SV	153.6 (50)	50.0 (15)		19.3 (5.8)			

Table 2. Comparision of experimental and theoretical total cross sections (in a_0^2) as a function of energy for the 3s to 3p transition in sodium. The experimental cross sections due to Buckman and Teubner (1979a), Enemark and Gallagher (1972) and Zapesochnyi et al (1975) are in the rows denoted BT, ZPA and EG respectively. The experimental error limits are enclosed in brackets under the cross section value.

E(eV)	10	20	22.1	54.4	100	150	217
FBA	255.0	169.3	158.6	84.0	52.9	38.4	28.5
CC2	165.1	134.7	128.9	77.7	50.9	37.5	28.1
CC4	138.5	123.0	118.9	75.3	50.0	36.9	27.8
FBA-CI	--	--	154.7	81.9	--	37.3	--
CC4-CI	--	--	115.9	73.2	--	36.3	--
BT				78.6 (11.6)	47.8 (6.9)	33.6 (5.0)	24.5 (3.5)
ZPA	188 (15)	143 (12)	134 (11)	69 (5.5)	41.5 (3.4)	30.9 (2.5)	23.8 (1.9)
EG	114.7 (5.0)	103.2 (4.2)	100.5 (4.2)	67.4 (2.0)	47.1 (0.6)	34.9 (0.3)	26.4 (0.3)

FIGURE CAPTIONS

Figure 1. Elastic differential cross sections for electron-sodium scattering at energies of 10 and 20 eV. The normalised cross sections of Gehenn and Reichert (1972) ▲ and the absolute cross sections of Srivastava and Vušković (1980) × are depicted. The theoretical results depicted are the results of a static-exchange calculation (SE), and two-(CC2) and four-(CC4) channel close-coupling calculations.

Figure 2. Elastic differential cross sections for electron-sodium scattering at energies of 54.4, 100 and 150 eV. The experimental cross sections of Buckman (1979) ● and the data of Srivastava and Vušković (1980) × are shown. The present SE, CC2 and CC4 cross sections and the second order optical potential model of Teubner et al (1978, TBN are shown.

Figure 3. Elastic differential cross sections for electron-neon scattering at energies of 100 and 150 eV. The results of a static-exchange SE and a two-channel R-matrix calculation by Fon and Berrington (1981) FB are depicted. Also shown are the experimental cross sections of Williams and Crowe (1975) ● and Gupta and Rees (1975a, b) ▲ .

Figure 4. Elastic differential cross sections for electron scattering from sodium and neon at 150 eV. The data of Buckman (1979) ● and of Gupta and Rees (1975b) ▲ are shown.

Figure 5 Small-angle differential cross sections for the 3s to 3p transition in sodium at energies of 22.1, 54.4, 100 and 150 eV. The theoretical cross sections shown are the result of the FBA, CC2 and CC4 calculations. The experimental results are taken from Buckman and Teubner (1979a) ● and Teubner et al (1986) ● .

Figure 6. Differential cross sections for the 3s to 3p transition in sodium at energies of 10, 20 and 22.1 eV. Also depicted are the experimental results of Teubner et al (1986) ● and Srivastava and Vušković (1980) ✗ .

Figure 7. Differential cross sections for the 3s to 3p transition in sodium at energies of 54.4, 100, 150 eV. The experimental results of Buckman and Teubner (1979a) ● and Srivastava and Vušković (1980) ✗ are shown.

Figure 8. Comparison of experimental and theoretical determinations of the parameter P_1 at energies of 12.1, 22.1 and 30 eV. Experimental data points from electron-photon coincidence experiments of the Flinders University group● (data points calculated from P_4 ▲) and the superelastic experiment of Hermann et al (1977) ✗ are shown. Results of the FBA, CC2 and CC4 calculations are appropriately labelled. Also depicted are values for P_1 (denoted <CC4>) that result when the CC4 calculation is convoluted (eq. 31) with a function roughly representing the angular acceptance of the apparatus.

Figure 9. Comparison of experimental and theoretical determinations of the parameter P_1 at energies of 54.4, and 100 eV. The only experimental data come from the electron photon coincidence experiments of the Flinders University group. Results of the CC2 and CC4 calculations are shown

Also depicted are values for P_1 (denoted <CC4>) that result when the CC4 calculation is convoluted (eq. 31) with a function roughly representing the angular acceptance of the apparatus.

Figure 10. Comparison of experimental and theoretical determinations of the parameter P_2 at energies of 12.1, 22.1 and 100 eV. Data from electron-photon coincidence experiments of the Flinders group● and the superelastic experiment of Hermann et al (1977) ✕ are depicted. Results of FBA, CC2 and CC4 calculations are appropriately labelled. Also depicted are values for P_2 (denoted <CC4>) that result when the CC4 calculation is convoluted (eq. 31) with a function roughly representing the angular acceptance of the apparatus.

Figure 11. Comparison of experimental and theoretical determinations of the parameter P_3 at energies of 12.1, 22.1 and 100 eV. Data from the electron-photon experiments of the Flinders group ● ; and the superelastic experiment of Hermann et al (1980) ✕ are depicted. Results of the CC2 and CC4 calculations are appropriately labelled. The first Born approximation (without exchange) gives a value of $P_3 = 0$ for all scattering angles. Also depicted are values for P_3 (denoted <CC4>) that result when the CC4 calculation is convoluted (eq. 31) with a function roughly representing the angular acceptance of the apparatus.

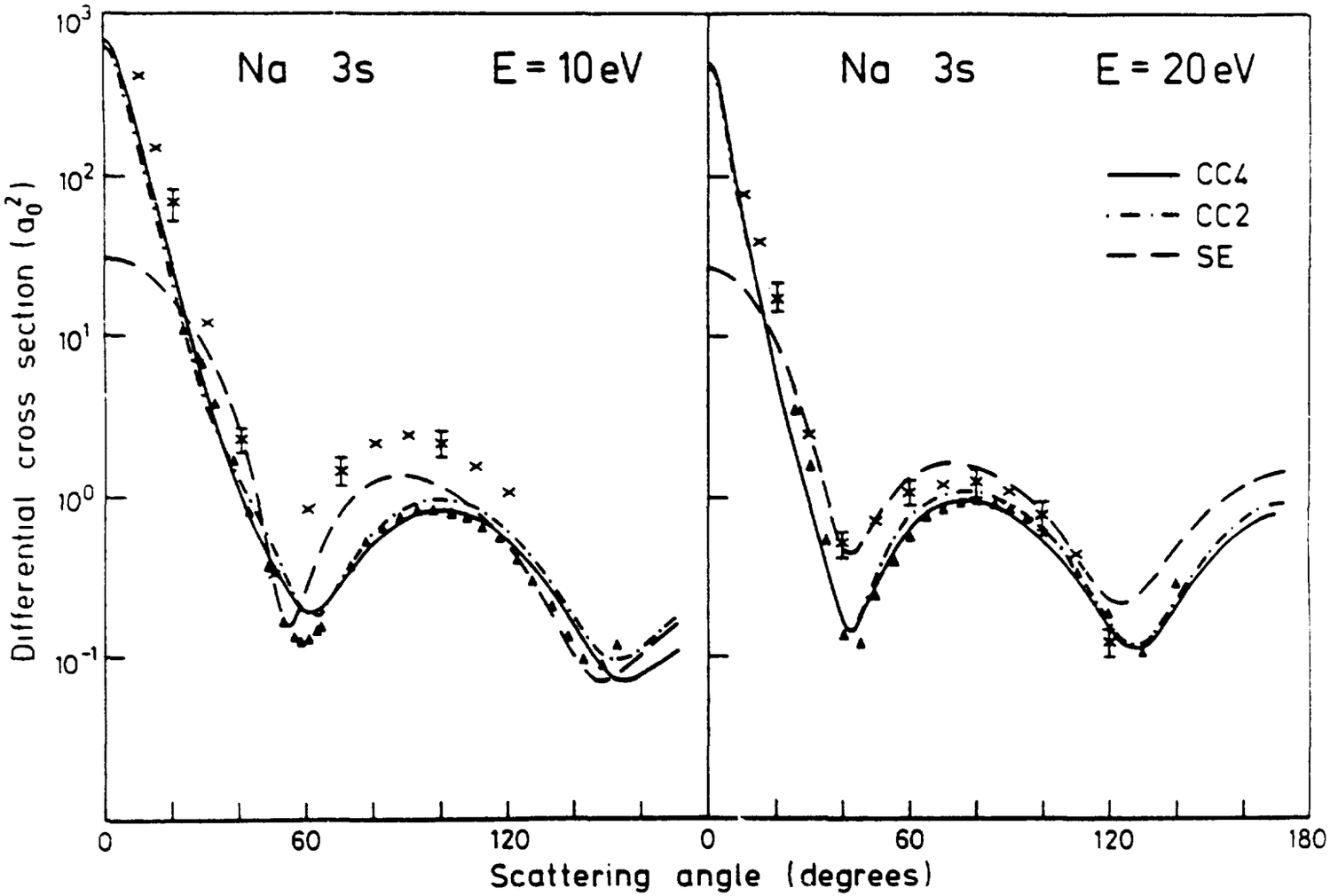
Na 3s E = 10 eV
Na 3s E = 20 eV
CC4
CC2
SE
Differential cross section (a_0^2)
10^3
10^2
10^1
10^0
10^{-1}
0
60
120
0
60
120
180
Scattering angle (degrees)

Fig. 1

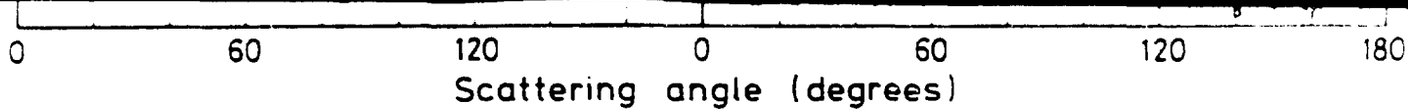
0
60
120
0
60
120
180
Scattering angle (degrees)

Fig. 1

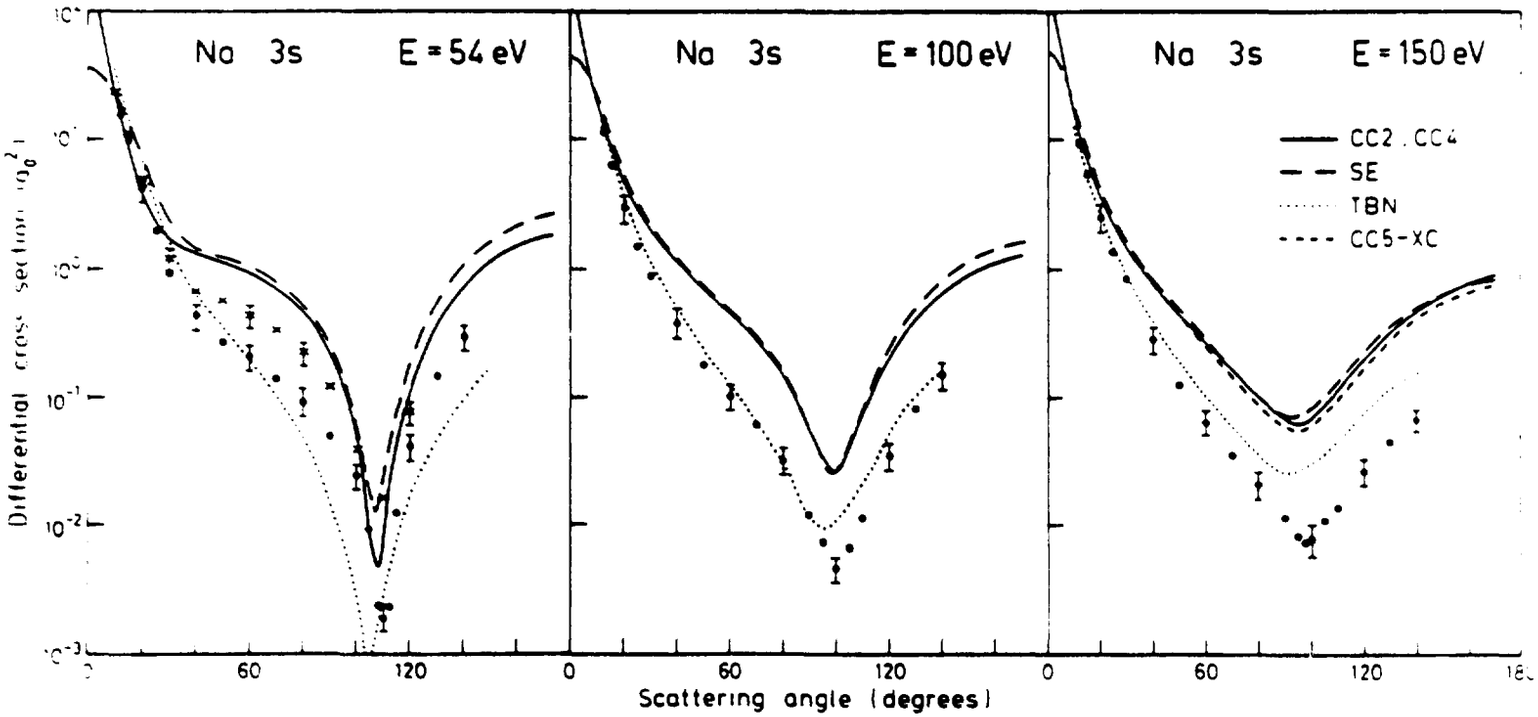
Na 3s E = 54 eV
Na 3s E = 100 eV
Na 3s E = 150 eV
CC2 . CC4
SE
TBN
CC5-XC
Scattering angle (degrees)

Fig. 2

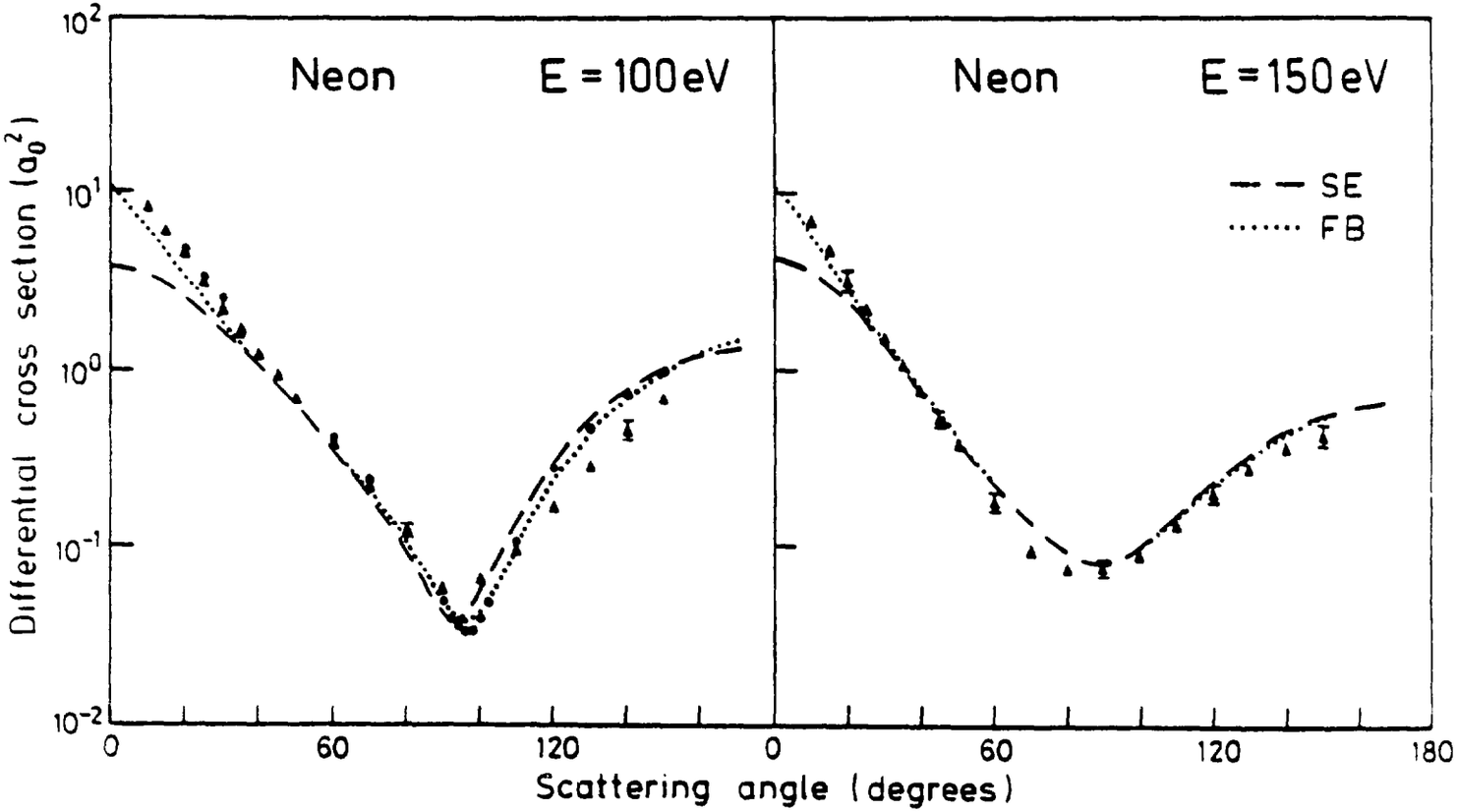

Fig. 3

Differential cross section (a_0^2)

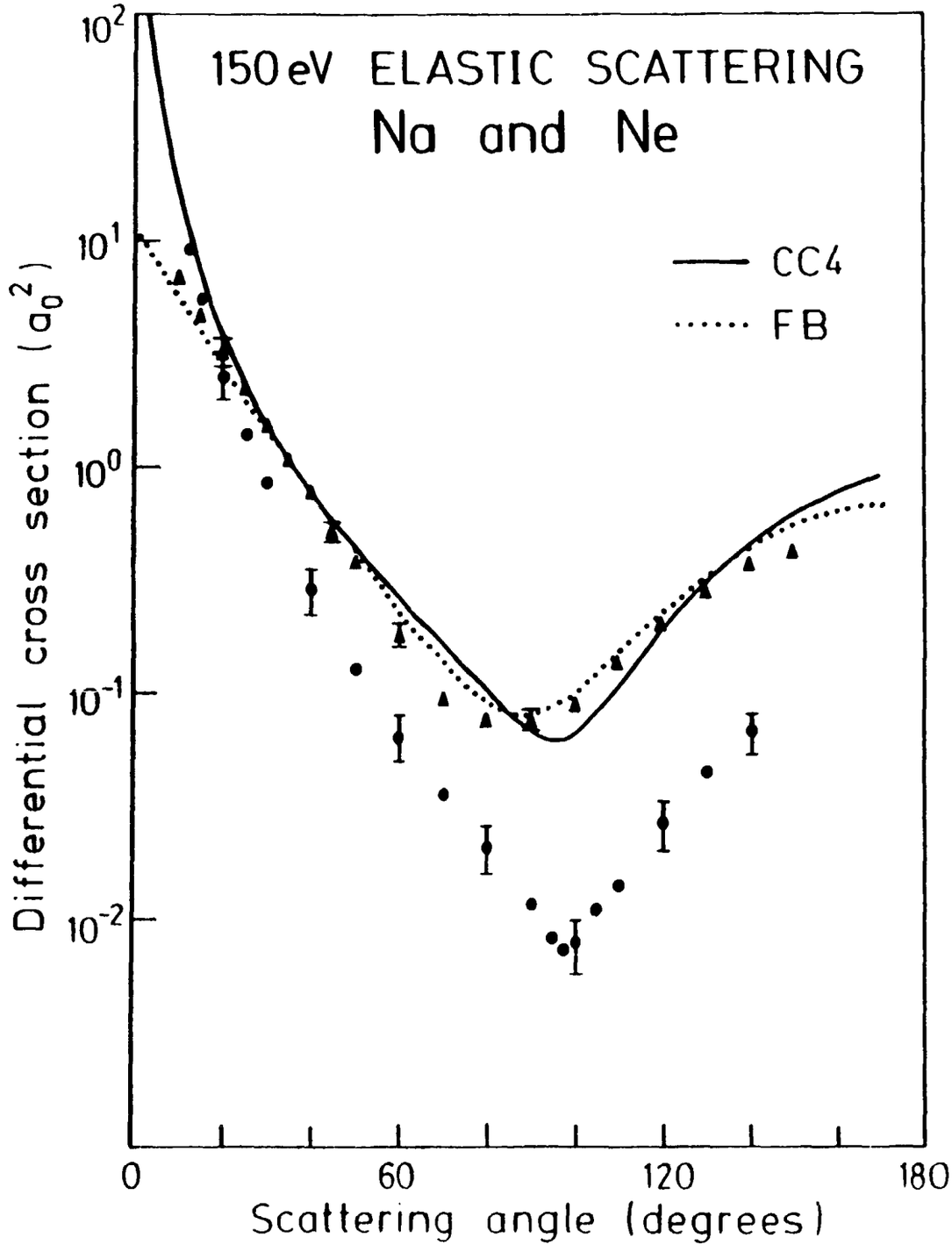
150 eV ELASTIC SCATTERING
Na and Ne
CC4
FB
Differential cross section (a_0^2)
10^2
10^1
10^0
10^{-1}
10^{-2}
0
60
120
180
Scattering angle (degrees)

Fig. 4

Fig. 3

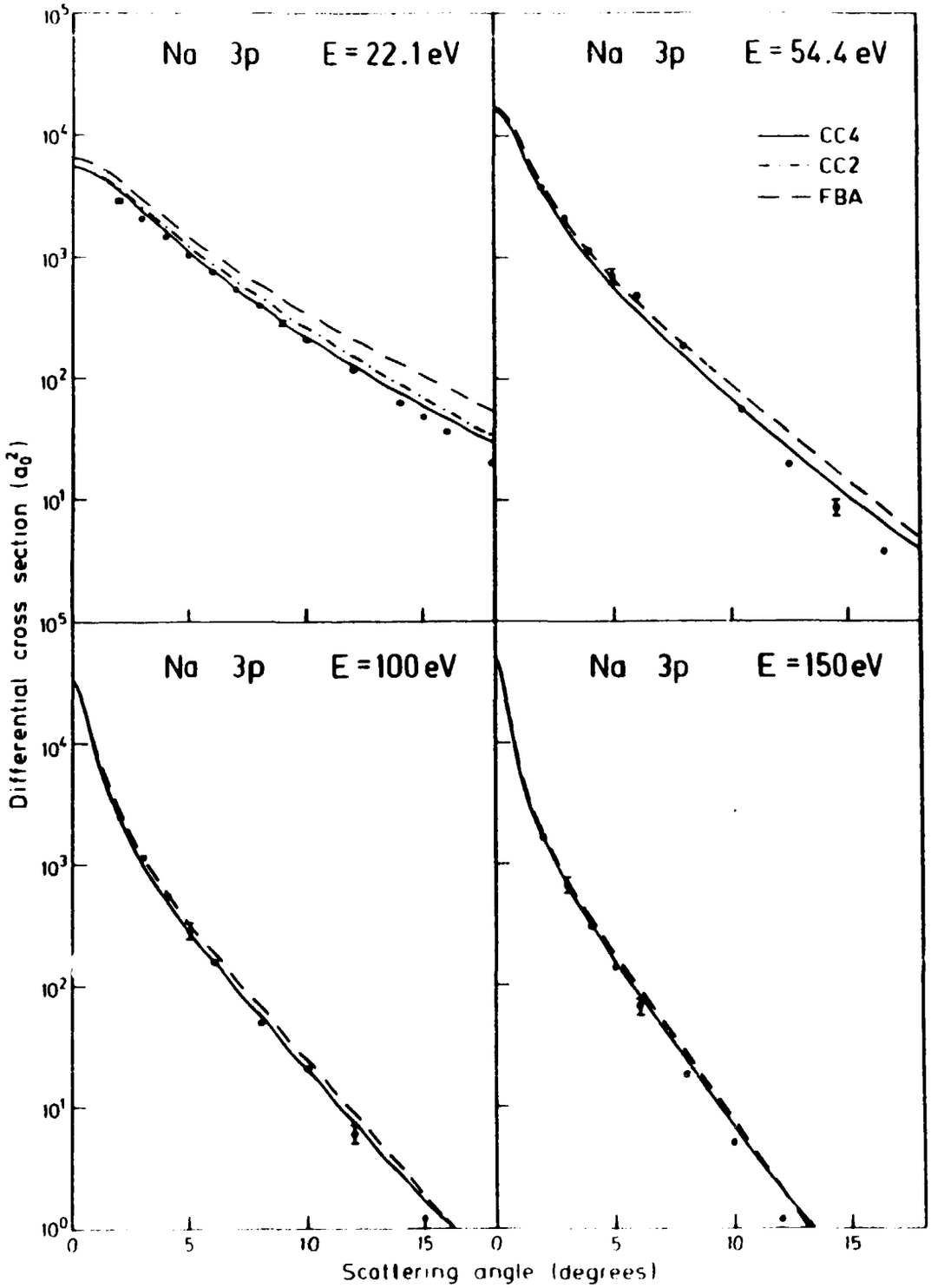
Na 3p E = 22.1 eV
Na 3p E = 54.4 eV
Na 3p E = 100 eV
Na 3p E = 150 eV
CC4
CC2
FBA
Differential cross section (a_0^2)
Scattering angle (degrees)
10^5
10^4
10^3
10^2
10^1
10^0
0
5
10
15

Fig. 5

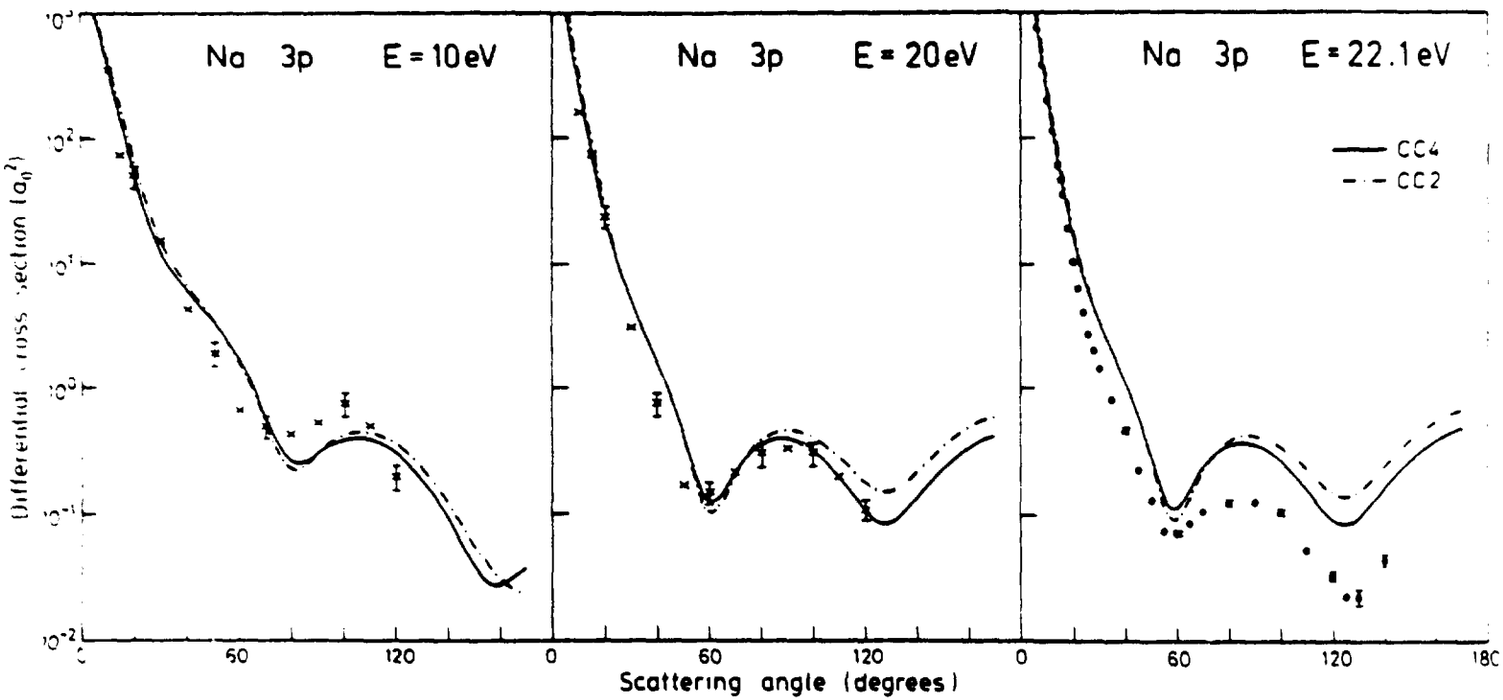
Na 3p E = 10eV
Na 3p E = 20eV
Na 3p E = 22.1eV
CC4
CC2
Differential cross section (a_0^2)
Scattering angle (degrees)
0
60
120
180

Fig. 6

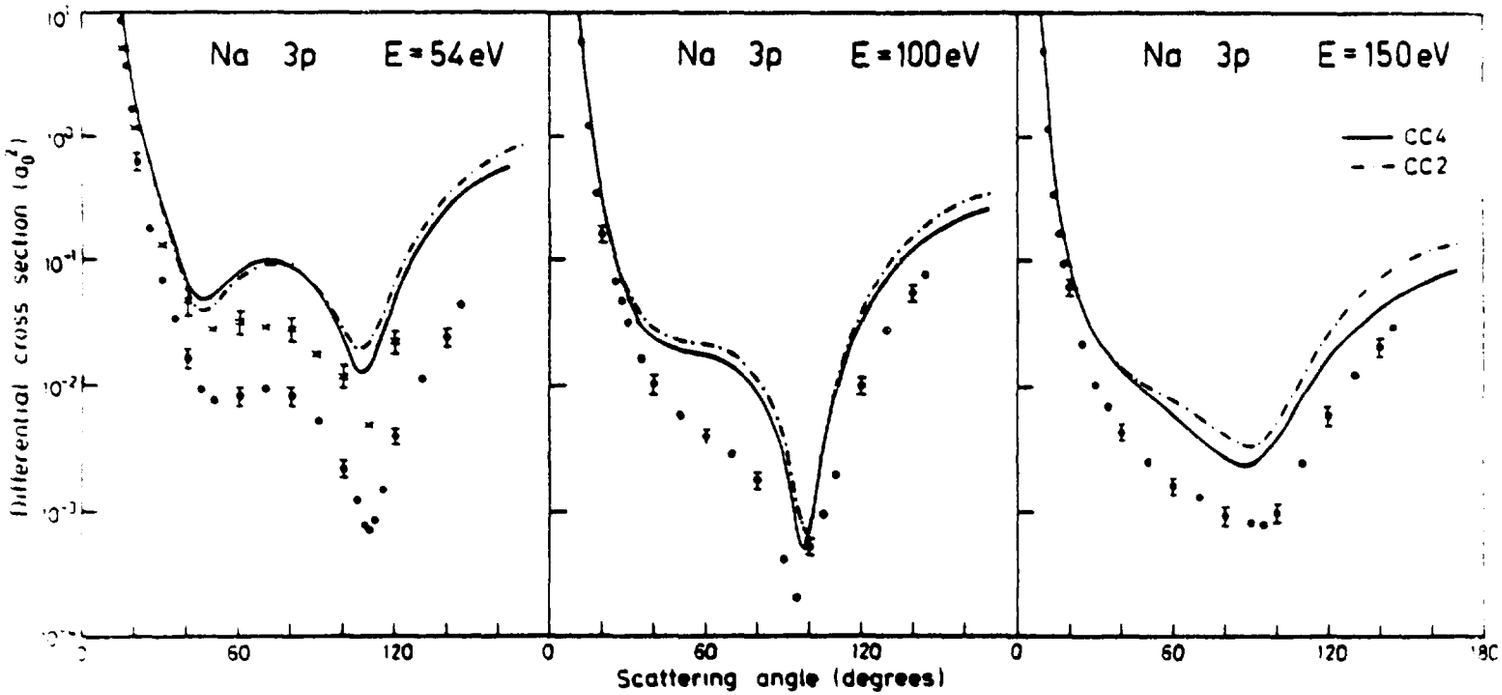
Na 3p E = 54 eV
Na 3p E = 100 eV
Na 3p E = 150 eV
CC4
CC2
Differential cross section (a_0^2)
Scattering angle (degrees)
0
60
120
180

Fig. 7

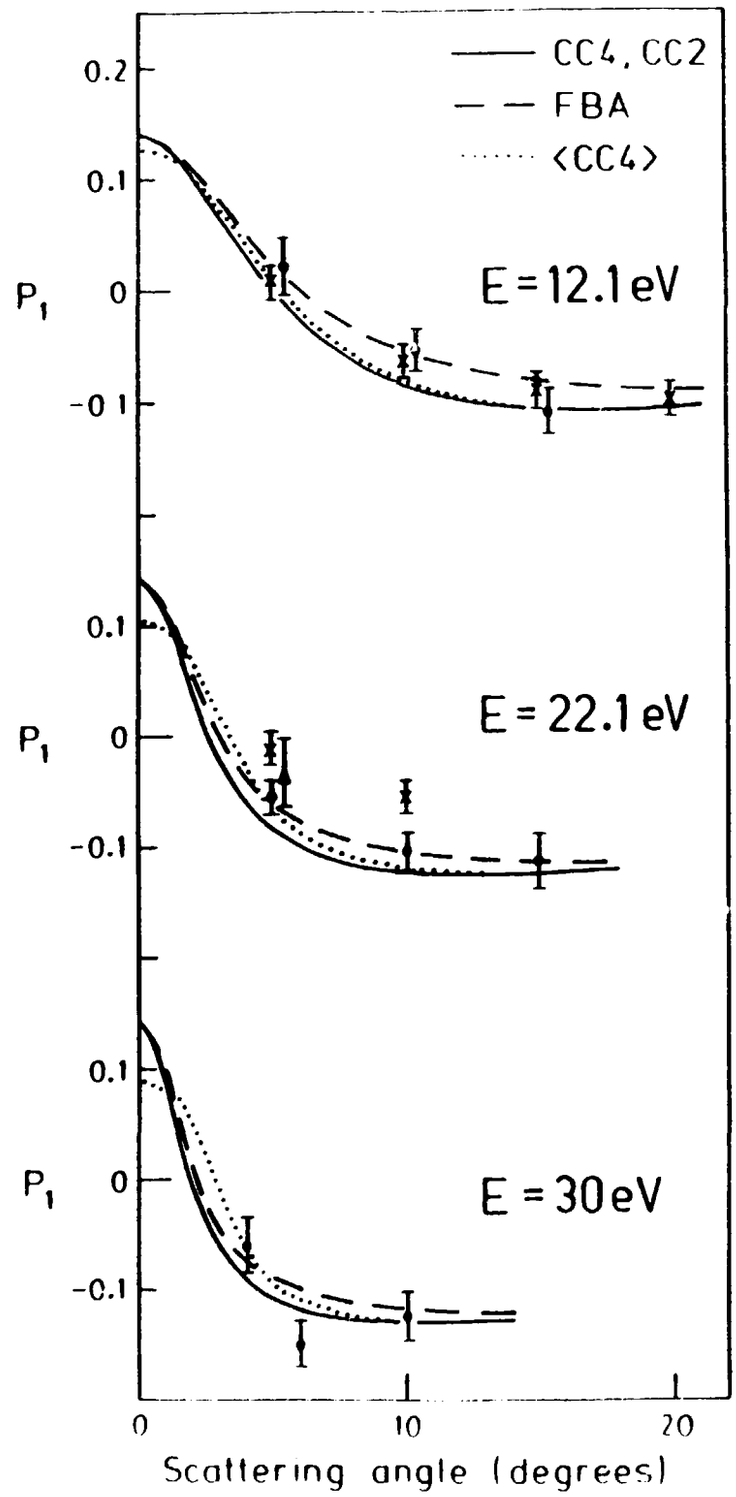
CC4, CC2
FBA
<CC4>
E = 12.1 eV
E = 22.1 eV
E = 30 eV
P1
0.2
0.1
0
-0.1
0
10
20
Scattering angle (degrees)

Fig. 8

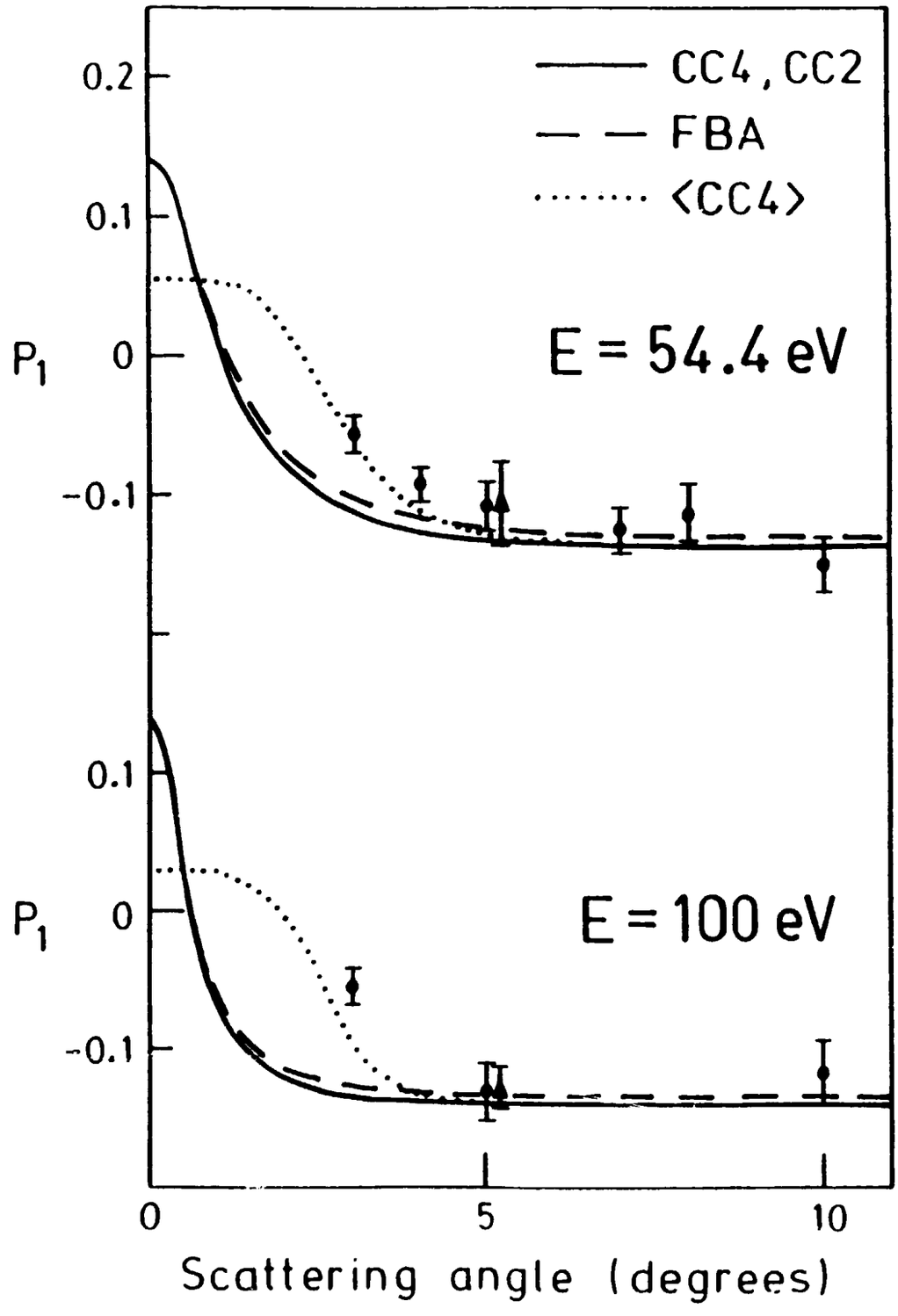
CC4, CC2
FBA
<CC4>
E = 54.4 eV
E = 100 eV
P_1
P_1
0.2
0.1
0
-0.1
0.1
0
-0.1
0
5
10
Scattering angle (degrees)

Fig. 9

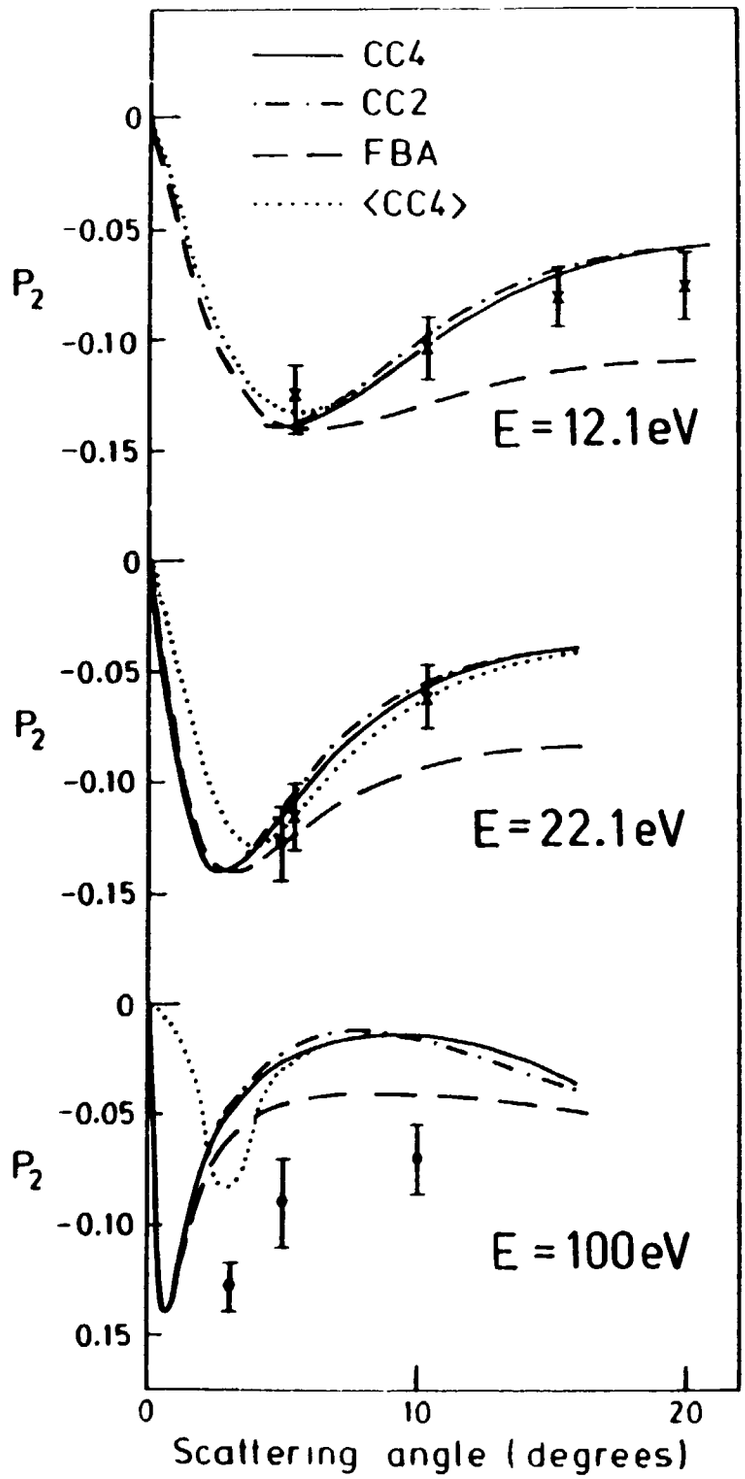
CC4
CC2
FBA
<CC4>
0
-0.05
-0.10
-0.15
P2
E = 12.1eV
E = 22.1eV
E = 100eV
0.15
0
10
20
Scattering angle (degrees)

Fig. 10

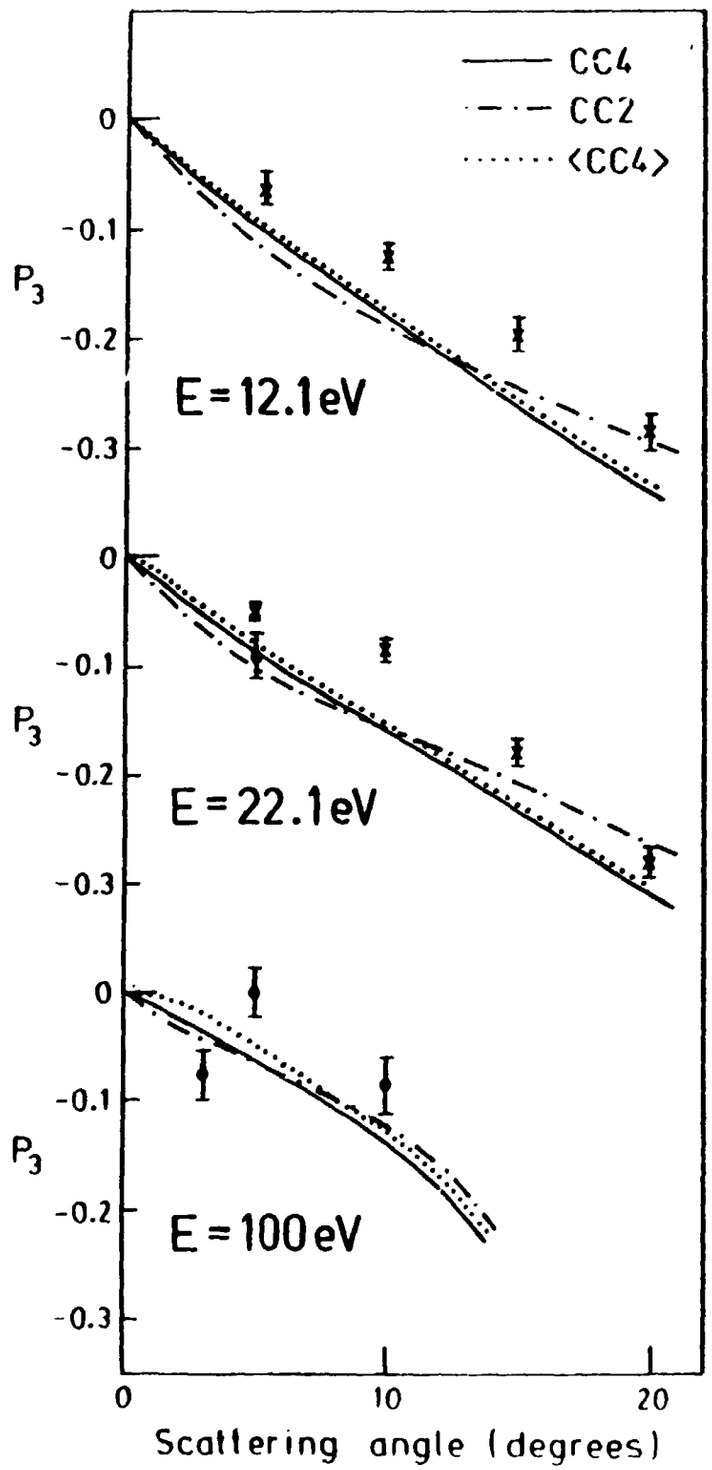
CC4
CC2
<CC4>
0
-0.1
-0.2
-0.3
P3
E=12.1eV
E=22.1eV
E=100eV
0
10
20
Scattering angle (degrees)

Fig. 11